Journal of Modern Optics
Publication details, including instructions for authors and subscription information:
http://www.tandfonline.com/loi/tmop20

# Light scattering on the $F = 1 \searrow F' = 0$ transition in a cold and high density $^{87}$Rb vapor

A.S. Sheremet[a], I.M. Sokolov[ab], D.V. Kupriyanov[a], S. Balik[c], A.L. Win[c] & M.D. Havey[c]
[a] Department of Theoretical Physics, State Polytechnic University, 195251, St.-Petersburg, Russia.
[b] Institute for Analytical Instrumentation,, RAS 198103, St.-Petersburg, Russia.
[c] Department of Physics, Old Dominion University, Norfolk, VA 23529, USA.
Published online: 10 Jan 2014.

To cite this article: A.S. Sheremet, I.M. Sokolov, D.V. Kupriyanov, S. Balik, A.L. Win & M.D. Havey , Journal of Modern Optics (2014): Light scattering on the $F = 1 \searrow F' = 0$ transition in a cold and high density $^{87}$Rb vapor, Journal of Modern Optics, DOI: 10.1080/09500340.2013.854419

To link to this article: http://dx.doi.org/10.1080/09500340.2013.854419

*Journal of Modern Optics*, 2014
http://dx.doi.org/10.1080/09500340.2013.854419

Taylor & Francis
Taylor & Francis Group

# Light scattering on the $F = 1 \rightarrow F' = 0$ transition in a cold and high density $^{87}$Rb vapor

A.S. Sheremet[a], I.M. Sokolov[a,b], D.V. Kupriyanov[a], S. Balik[c], A.L. Win[c] and M.D. Havey[c]*

[a]*Department of Theoretical Physics, State Polytechnic University, 195251, St.-Petersburg, Russia;* [b]*Institute for Analytical Instrumentation, RAS 198103, St.-Petersburg, Russia;* [c]*Department of Physics, Old Dominion University, Norfolk, VA 23529, USA*

(*Received 28 February 2013; accepted 8 October 2013*)

We report an experimental study of near resonance light scattering on the $F = 1 \rightarrow F' = 0$ component of the $D_2$ line in atomic $^{87}$Rb. Experiments are performed on spatially bi-Gaussian ultracold gas samples having peak densities ranging from about $5 \times 10^{12} - 5 \times 10^{13}$ atoms/cm$^3$ and for a range of resonance saturation parameters and detunings from atomic resonance. Time resolution of the scattered light intensity reveals the dynamics of light scattering, optical pumping, and saturation effects. The experimental line shape for optical excitation in steady state is found to be significantly narrower than that for the $^{87}$Rb $F = 2 \rightarrow F' = 3$ transition studied previously under similar conditions. This difference is qualitatively reproduced by a theoretical model of the two transitions at similar density.

**Keywords:** quantum optics; ultracold atomic physics; Anderson localization; radiation trapping; quantum memories



## 1. Introduction

The interaction of light with dense atomic gases is a vigorous area of research in quantum optics [1–24].[1] Part of this interest stems from the interdisciplinary nature of the field, and with the large number of fundamentally important results and potential applications that have emerged. Recent efforts have ranged from basic studies of light localization in disordered systems [25–33], including atomic gases, to investigation of cooperative scattering [34–41]. Areas of experimental and theoretical research with both fundamental motivations and possible applications include searches for atomic physics based random lasing [42–47] and quantum memories for quantum information and communications [48–50]. Single photon optical memories in dense atomic gases may potentially be derived from a number of approaches, including development of subradiant atomic-photonic modes [51], and extensions of electromagnetically-induced-transparency (EIT) based approaches to novel two-photon optical schemes at higher densities [7,9,10,18,19,52,53].

We have ongoing experimental and theoretical research efforts focused in part on developing quantum memories using either two-photon EIT based approaches on one hand [52–56], and on the possible formation of subradiant single photon modes on the other [27–29,57]. To obtain formation of subradiant modes is a challenging experimental enterprise, and requires atomic densities $\sim 10^{14}$ atoms/cm$^3$, in order to achieve high orders of multiple light scattering in the sample. In addition, dynamical processes which either dephase the multiply scattered light or which lead to reduction in the scattering cross-section should be well understood. The current program is focused on nearly optically closed hyperfine transitions associated with the $D_2$ transition in ultracold $^{87}$Rb. These transitions, being nearly closed, are the only ones suitable for multiple scattering studies in $^{87}$Rb. These two transitions are the $F = 2 \rightarrow F' = 3$ main optical trapping component and the $F = 1 \rightarrow F' = 0$ transition arising from the lower energy ground state hyperfine component. We have reported elsewhere our experimental research associated with light scattering on the $F = 2 \rightarrow F' = 3$ transition [58]. For these two transitions, and for similar density and temperature conditions, interactions among the atoms in the sample can differently affect the optical excitation line shape. An important aspect of the present paper is comparison of the line shapes for those two transitions, and to make similar comparisons between them using a theoretical model of the optical response of the systems.

In the present paper we report experimental investigation of the $F = 1 \rightarrow F' = 0$ transition in $^{87}$Rb. Overall, our studies include examination of the roles of atomic density, optical saturation, and detuning of probe radiation from optical resonance on the $F = 1 \rightarrow F' = 0$ transition. In the present paper, we concentrate primarily on steady

*Corresponding author. Email: mhavey@odu.edu

state optical excitation and how the light scattering signals depend in that case on probe detuning and atomic density. In the following sections we first provide some details of our experimental approach. This is followed by presentation of our experimental results and comparative discussion on the basis of theoretical models of the light scattering process.

## 2. Experimental configuration

A schematic diagram of the experimental apparatus used in the measurements is shown in Figure 1, while the particular optical transitions of interest associated with the atomic $^{87}$Rb $D_2$ line are shown in Figure 2. As illustrated in Figure 1, the central part of the experimental apparatus is a magneto optical trap (MOT) which serves to form and confine cold $^{87}$Rb atom samples. The MOT is a standard vapor-loaded trap formed in a vacuum chamber with a base pressure $\sim 10^{-9}$ torr. The six MOT beams are derived from a single external cavity diode laser (ECDL) with the grating arranged in a Littrow configuration. The main master diode laser is frequency locked to a saturation absorption feature produced in a room temperature Rb vapor cell. The master laser power is increased by injecting the master output into the slave laser. The arrangement provides more than 20 mW of trapping light in laser beams of cross-sectional area $\sim 2\,\mathrm{cm}^2$. The slave laser output is switched and spectrally shifted as required with an acousto optical modulator (AOM) to a frequency set at about 18 MHz below the $^{87}$Rb $F = 2 \rightarrow F' = 3$ trapping transition. The repumper laser is also an ECDL of the same basic design as the main MOT laser, and is locked to the $F = 1 \rightarrow F' = 2$ hyperfine transition. The repumper delivers a beam of maximum intensity $\sim 0.6\,\mathrm{mW\,cm}^{-2}$ and is delivered along the same optical path as the main trapping laser beams. Switching of the repumper laser is also controlled with an AOM.

In the experiments reported here, the cold atom sample is initially produced in the higher energy $F = 2$ level. Direct absorption imaging measurements of the peak optical depth

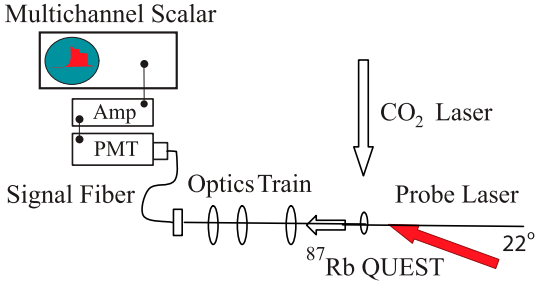


Figure 1. Schematic diagram of the experimental apparatus. In the figure, PMT refers to an infrared sensitive photomultiplier tube and Amp refers to a fast preamplifier. MOT stands for magneto optical trap, while QUEST is an abbreviation for quasi electrostatic trap. (The colour version of this figure is included in the online version of the journal.)

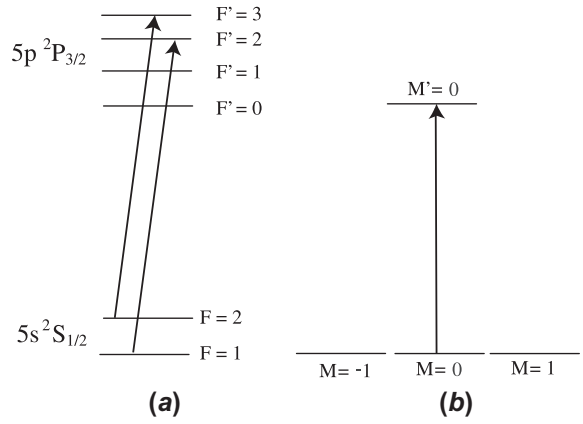


Figure 2. Energy level diagrams illustrating the experimental scheme. (*a*) The MOT and repumping transitions used in the present experiment. (*b*) Probe excitation with linearly polarized light ($z$-direction) used in the present experiment. In part (*b*) of the figure, the Zeeman levels have been broken out to show the role of Zeeman optical pumping out of the $F = 1$, $M = 0$ state to the $F = 1$, $M = \pm 1$ states.

on the $F = 2 \rightarrow F' = 3$ transition yielded, for this sample, $b_o \sim 10$ in a Gaussian radius of $r_o \sim 0.45$ mm. However, the main sample production goal is to transfer a significant number of the trapped atoms to a carbon-dioxide laser ($CO_2$) based far off resonance optical dipole trap. The 100 W $CO_2$ laser based trap operates at a wavelength of 10.6 μm and is deeply in the quasistatic trapping regime. This laser is focussed to a radial spot size of $\sim 55\,\mu$m, and a corresponding Rayleigh range of $z_R \sim 750\,\mu$m. The $CO_2$ laser focal zone is overlapped with the MOT trapping region, while application of the laser beam itself is controlled by a 40 MHz AOM. The atom sample formed in the MOT is compressed and loaded into the quasistatic dipole trap (QUEST) by detuning the MOT master laser 60 MHz to the low frequency side of the trapping transition, while simultaneously lowering the repumper intensity over an order of magnitude. The resulting temporal dark spot MOT loads the atoms predominantly into the lower energy $F = 1$ hyperfine component. The result of this procedure is transfer of about 15% of the MOT atoms to the QUEST. It is important to note that this transfer efficiency is determined after a QUEST holding period of about 1 s, during which the atomic sample naturally evolves towards thermal equilibrium (this happens through elastic collisions between the confined Rb atoms). Auxiliary measurements of the QUEST principal characteristics after the 1 s hold period, by absorption imaging, parametric resonance [59], and the measured number of atoms transferred show a sample with peak density about $5 \times 10^{13}$ atoms/cm$^3$ and a temperature of $\sim 65\,\mu$K. The 1/e lifetime of the confined atoms is longer than 5 s, and is limited by background gas collisions. The residual magnetic field in the sample area, when the MOT quadrupole field is switched off, is estimated to be less than a few mG.

Table 1. QUEST parameters relating the peak transverse optical depth on the $F = 1 \rightarrow F' = 0$ transition to the maximum sample density and the Gaussian radii of the atomic cloud.

| Peak $b_t$ | $n_o$ (atoms/cm$^3$) | $r_o$ ($\mu$m) | $z_o$ ($\mu$m) |
|---|---|---|---|
| 40 | $5.0 \times 10^{13}$ | 9.8 | 248 |
| 28 | $2.5 \times 10^{13}$ | 13.8 | 248 |
| 20 | $1.2 \times 10^{13}$ | 19.5 | 248 |
| 13 | $5.1 \times 10^{12}$ | 30.4 | 249 |

In the main experimental protocol, a probe beam tuned in the spectral vicinity of the $F = 1 \rightarrow F' = 0$ nearly closed transition is directed towards the sample, and the resulting scattered light signals collected as illustrated schematically in Figure 1. The probe laser is of the same design as the repumper laser, has a bandwidth $\sim 3$ MHz, and is switched and directed by an acousto optical modulator towards the sample. Because of constraints on the vacuum chamber geometry, the linearly polarized probe beam is directed (see Figure 1) at an angle of approximately 30° away from the fluorescence collection direction. The probe beam is also directed downwards towards the sample at an angle of 22.5° (as shown in Figure 1). Finally, the sample fluorescence is collected without regard to light polarization; as light scattering is dominated by the $F = 1 \rightarrow F' = 0$ transition we expect the scattered light to be mainly unpolarized (very small contributions from the quite far off resonance $F = 1 \rightarrow F' = 1, 2$ transitions are in general polarized in the single scattering limit).

To close this section, we point out that in some of the experiments reported here the atomic density was varied over a factor of about 10. This was accomplished by allowing for a period of ballistic expansion of the cloud after the QUEST was turned off. The atomic sample temperature is known (by ballistic expansion measurements), so this procedure allows the peak density or the peak optical depth to be determined. As the sample is well approximated by a two-axis Gaussian atom distribution,[2] the two Gaussian radii and the peak atom density (or the total number of atoms in the sample), are sufficient to determine the two peak optical depths characterizing the sample. We summarize in Table 1 the peak transverse optical depth $b_t$ the peak atom density at the center of the sample $n_o$, the transverse Gaussian radius $r_o$, and the longitudinal Gaussian radius $z_o$. The optical depth refers here to that of the nearly closed $F = 1 \rightarrow F' = 0$ hyperfine transition, which has a total resonance light scattering cross-section of $3.23 \times 10^{-10}$ cm$^2$.

## 3. Results and discussion

In this section we present results associated with on-resonance light scattering, where on-resonance refers to the bare-atom $F = 1 \rightarrow F' = 0$ hyperfine resonance frequency, and with variations around that frequency. We emphasize that the measurements are made at a fixed single angle with respect to the incident probe laser; the geometrical setup is described in the previous section. With this in mind, we first expect that the scattered light will be unpolarized, as the excited level has $F' = 0$. However, because of the high optical depth of the sample, the scattered light intensity should show important angular dependence [29,54,60]. For instance, light scattered in the near forward direction shows a minimum in the spectral variations near the resonance line center. This can effect the time evolution of the scattered light signals as well [54]. On the other hand, light scattered in the backwards direction shows an enhancement due to the coherent backscattering effect. This spatially cone shaped feature depends critically on probe laser intensities near saturation and also on the spectral detuning from atomic resonance.

### 3.1. *On-resonance scattering*

We start by presenting in Figure 3 the results of typical measurements of the time dependence of light scattered from the atomic sample. These measurements are made for a maximum density sample, which in this case has a transverse optical depth of $b_t \sim 40$, and a peak atom density at the center of the sample of $5.0 \times 10^{13}$ atoms/cm$^3$. These measurements are made for a range of probe laser intensities, which for the most part are well below the saturation intensity $I_{sat} \sim 14$ mW cm$^{-2}$ for linearly polarized excitation of the $F = 1 \rightarrow F' = 0$ transition. We see for higher probe laser intensities a quite rapid build up to a peak intensity followed by a decay of about 1 $\mu$s to a steady state. The build up time is less than about 100 ns, and is limited by the turn-on time of the switching AOM used to control application of the probe laser to the sample. We also note that as the probe laser intensity is reduced, the transient peak is reduced, and for the lowest probe laser intensities the scattering signal smoothly rises to a steady value. The overall behavior is summarized in Figure 4, where the nearly linear growth of the peak in the scattering signal, and the leveling off of the steady state signal is shown. This general behavior of the transient response and the variations of the response with probe laser intensity was found to be qualitatively the same for a range of densities from $0.1 n_o$ up to the peak density $n_o$ (see Table 1). As the maximum laser intensity used in these experiments is well below the optical saturation intensity, we can understand the transient behavior to result from Zeeman optical pumping in the ground level due to elastic Raman transitions to the $F = 1, M = \pm 1$ states. This optical pumping does not completely deplete the $F = 1, M = 0$ state because multiple elastic light scattering allows for a build up of radiation within the atomic sample. This gives rise to optical pumping by the diffuse light in the sample, which competes with direct Zeeman optical pumping by the probe beam and results in a nonzero steady state level for the scattered

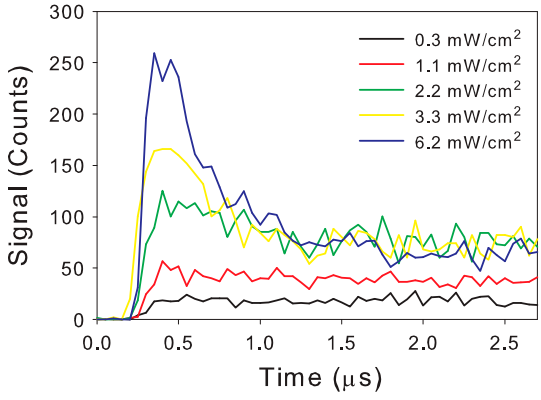


Figure 3. Time evolution of the probe scattered light intensity on the $F = 1 \rightarrow F' = 0$ hyperfine transition. The atomic density is at its peak level for these measurements. Signals are shown for several different probe laser intensities. The role of optical pumping is apparent at the larger probe intensities. Probe detuning from resonance $\Delta = 0$. (The colour version of this figure is included in the online version of the journal.)

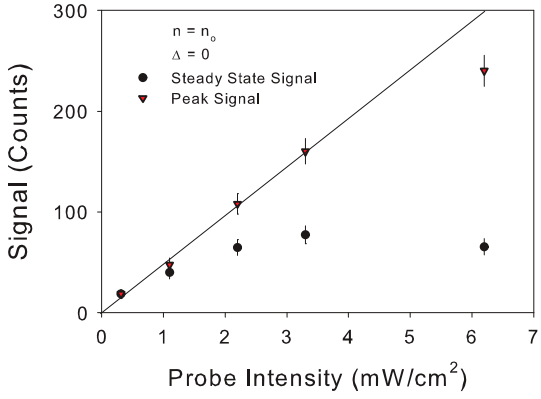


Figure 4. Variation of the peak and steady state signal levels as a function of the probe laser intensity. Atomic density is at is maximum value $n_o$ for these data. Probe detuning from resonance $\Delta = 0$. (The colour version of this figure is included in the online version of the journal.)

light signal as seen in Figures 3 and 4. This process as considered for a wide range of densities and laser intensities will be treated in a later report. In the present paper we are concerned with the steady state signals for the case where the probe intensity is so weak, and the number of scattered photons so few, that there is no mesoscopic rearrangement of populations in the $F = 1$ level during realization of a single sample. The main results of this paper, as presented in this and the following section, are recorded under those conditions.

We present in Figure 5 measurements of the variation of the total scattered light intensity from the $F = 1 \rightarrow F' = 0$ hyperfine transition as a function of systematic changes in the atomic density. These measurements were made at very low probe laser intensity, under conditions selected so that there was no perceptible optical pumping, as in

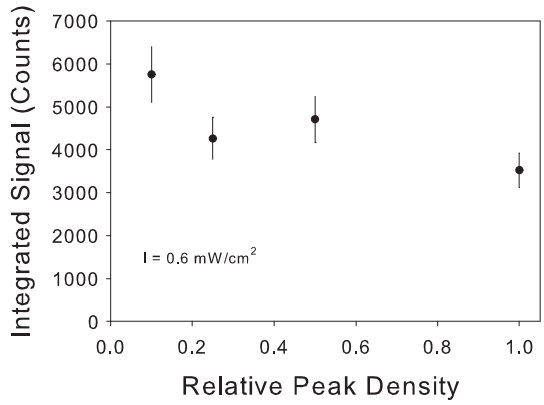


Figure 5. Variation of the total scattered signal intensity due to systematic changes in the atomic density. Probe detuning from resonance $\Delta = 0$.

the lowest intensity results shown in Figures 3 and 4. In Figure 5 we see that as the density decreases, the overall intensity of the scattered light increases. A similar behavior [58,60] has been observed for measurements on the $F = 2 \rightarrow F' = 3$ hyperfine transition of $^{87}$Rb. The effect is due to the collective nature of near resonance light scattering from a high density and cold atomic gas. Because the optical depth is so large for the highest density, light scattering occurs primarily from the outer surface of the sample. Relatively few atoms then contribute to the signal. For lower density the light can penetrate more deeply and a relatively larger number of atoms participate, leading to a larger signal. In a previous paper we have obtained the general scaling law for such a situation [60]. The scaling obtained there reflects the fact that for fixed detuning, and for a fixed total number of atoms, the scattered light intensity scales at high density in proportion to the effective area of the atomic sample.

### 3.2. *Variations with spectral detuning from resonance*

We now consider the variations of the scattered light signals as a function of detuning of the probe laser frequency from bare atomic resonance, where $\Delta = 0$. These data are recorded under conditions of a very weak probe laser, so that Zeeman optical pumping is negligible. For the steady state regime (as in the lowest probe intensity results of Figure 3), this dependence is shown in Figure 6. There we see that the spectral variations show a clear resonance behavior in a range of 3 to 4 $\gamma$ about $\Delta = 0$, where $\gamma$ is the $\sim 6$ MHz natural width of the atomic resonance. The solid line is a Lorentzian line profile, which well describes the resonance line shape, and yields a full width at half maximum of slightly larger than 10 MHz. A full-width greater than the natural width is expected, due to the high optical depth of the sample and due to the dipole–dipole interaction of the atoms under high density conditions. Selection of the

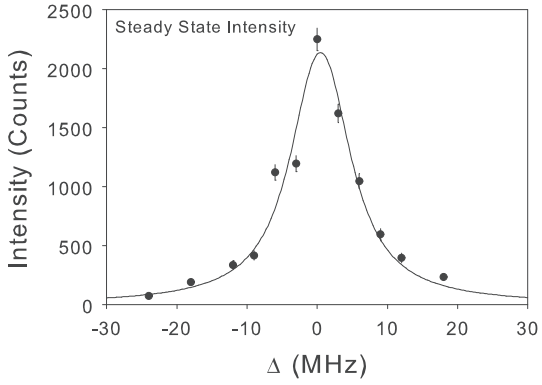


Figure 6. Near-resonance spectral variation of the total scattered light intensity in the spectral vicinity of the $F = 1 \rightarrow F' = 0$ hyperfine transition.

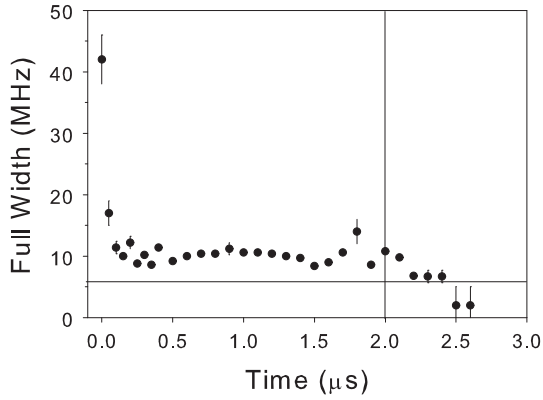


Figure 7. Time evolution of the probe scattered light intensity on the $F = 1 \rightarrow F' = 0$ hyperfine transition. The atomic density is at its peak level for these measurements.



Lorentzian line shape is arbitrary, but gives a decent fit to the data and a consistent way of estimating the full width under different experimental conditions. Within the spread of the data, a fit using a Gaussian line profile yields essentially the same full width at half maximum. The physical origin of the determined line shape is the balance between optical excitation of the various modes of the system in competition with the decay of those modes. In steady state, we expect a distribution of those modes to contribute to the measured line shape [58]. We emphasize here that the width of the response in Figure 8 (see Section 4) is significantly less than that in our earlier measurements [58] on the $F = 2 \rightarrow F' = 3$ transition. This highlights one of the main points in this paper; there is different manifestation of the dipole–dipole interaction, at higher atomic densities, between the atoms for differently degenerate electronic transitions.

To further analyze the experimental data, we have extracted the full width at half maximum of the spectral profile as a function of time [58]. With reference to the lowest intensity results of Figure 3, this is equivalent to making a slice on the time axis of 100 ns and recording the spectral profile as a function of detuning in this time window. Repeating this procedure for the full sequence of data over the 2.5 μs range of the probe excitation and decay signals yields the excitation spectrum shown in Figure 7. There we see that the line width is large for very short times, rapidly decays to its steady state level (as in Figure 6), and then sharply decreases again after the probe pulse is extinguished. For the shortest-time turn on of the excitation pulse, for time scales on the order of the Wigner scattering time, single scattering dominates, and the line width can be estimated to be $\Delta_o = \gamma/2(b_o - 1)^{1/2}$, where $b_o$ is the on resonance transverse optical depth through the center of the cloud [58]. This physical situation persists only for the shortest times. For the experiments reported here $b_o = 40$, giving a full width of $\Delta_o = \gamma(b_o - 1)^{1/2} \sim 37$ MHz, in good agreement with the short time value of Figure 7.

Upon turn off of the probe pulse the spectral width of the excitation spectrum decreases from its steady state value of about 10 MHz to a value on the order of the natural width. As in the spectral response upon turn-on of the probe pulse, the line shape here is also well fit by a Lorentzian form. However, we point out that the spectral width of the probe laser itself is about 1 MHz, and has a measured Gaussian power spectrum. This means that the widths determined by these measurements are slightly larger than that determined by the physical processes involved. In fact, the longest lived mode [58] for these samples corresponds to the so-called Holstein mode, or the longest lived diffusive mode for the sample under study; the lifetime of this mode can be significantly smaller than the natural width of the transition. Such a long lived mode would manifest itself in the long-time afterglow of the atomic sample, following optical excitation.

## 4. Theory

In this section we present theoretical calculations of the steady state line shape for optical excitation of the $F = 1 \rightarrow F' = 0$ hyperfine transition. We have observed previously, and reported in this paper, that the steady state excitation spectrum for the two closed transitions out of the hyperfine ground levels of $^{87}$Rb have quite different steady state line widths. Here we then wish to compare the results of theory calculations with previous ones associated with the $F = 2 \rightarrow F' = 3$ transition. In comparison of the pair of experimental results and the pair of theoretical ones, we aim to obtain some physical insight into the differences between the manifestations of the differently degenerate transitions on the line shapes.

The self-consistent approach accepts the description of the scattering problem on the level of the macroscopic (i.e. mesoscopically averaged) Maxwell theory, where the dielectric susceptibility obeys an equation resulting from the self-consistent dynamics of the driving (probe) field and of the atomic dipoles. The crucial assumption is that groups of closely located atomic dipoles respond to the field cooperatively such that the longitudinal dipole–dipole interaction can be incorporated into the Lorentz–Lorenz local-

field correction. For a low intensity of the driving field (where optical pumping can be neglected) the atoms equally populate the Zeeman sublevels and the medium is isotropic and can be parameterized by a single dielectric constant. If the atoms are homogeneously distributed in a spherical volume, then it is possible to express the scattering cross-section by the standard solution of the Debye–Mie problem. In Figure 8 we reproduce the spectral dependencies of the total cross-section calculated for such a spherically symmetrical atomic system. Here we remind the reader that all values of the atomic density in this section are expressed in units of $(\lambda/2\pi)^{-3}$. We use the densities essentially less than in the peak point of the cloud to emphasize the importance of the contribution from the tail area of the Gaussian distribution in the experimental observation of the scattering process. The plotted dependencies demonstrate the smoothed spectral profile with a bandwidth qualitatively in agreement with the experimental data of Figure 6. Note that there is a slight asymmetry in the spectral behavior related with the density effects which is a consequence of the spectral asymmetry of the dielectric permittivity. Because of the essential differences in geometries of this model and the experiment, which is a prolate double Gaussian distribution in experiment and spherically homogeneous in theory, we cannot make direct quantitative comparison of experimental and theoretical results but we can point out at least the qualitative agreement between both the data sets.

The results in Figure 8, obtained for the $F = 1 \rightarrow F' = 0$ hyperfine transition of $^{87}$Rb should be compared to those reported in our previous publications [27,58,60] on the $F = 2 \rightarrow F' = 3$ hyperfine transition of the same atom. We can see in these cases that the steady state line shapes at nearly identical experimental densities, where the atomic separations on the average are nearly the same, are quite different. Of particular interest is the width of the transitions, which is significantly narrower for the $F = 1 \rightarrow F' = 0$ transition than the $F = 2 \rightarrow F' = 3$ transition. This important difference is due to the different manifestation of the dipole–dipole interaction, at higher atomic densities, between the atoms for differently degenerate electronic transitions.

Finally, we discuss microscopic calculations for the cooperative scattering process for a macroscopic collection of atoms with a degenerate ground state. This calculation is rather difficult because of the rapidly rising number of equations to be solved $d_e N d_g^{N-1}$, where $d_e$ is the degeneracy of the atomic excited state and $d_g$ is the degeneracy of the ground state. Here $N$ is the number of atoms considered in the calculations. This makes practically very difficult exact microscopic calculations for the scattering process and for its time-dependent fluorescence dynamics. In this section we present the results of our calculations of the scattering spectrum in the steady state regime.

As we mentioned, the microscopic calculations can be only approximately done for the considered transition. Here we reproduce the results of our calculations based on the

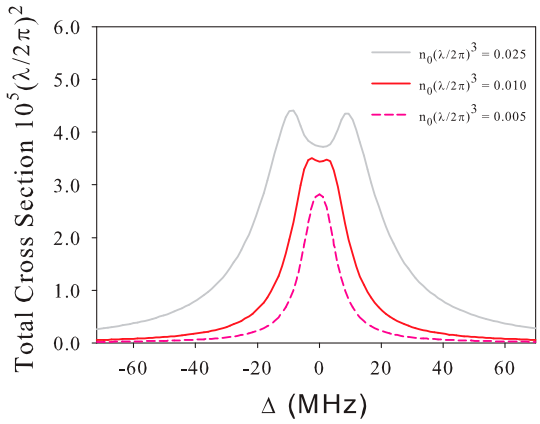


Figure 8. The scattering cross-section calculated in the Debye–Mie model for an atomic sample with radius 30 μm. Atoms fill a sphere homogenously with the density varying from 0.005 to 0.025. (The colour version of this figure is included in the online version of the journal.)

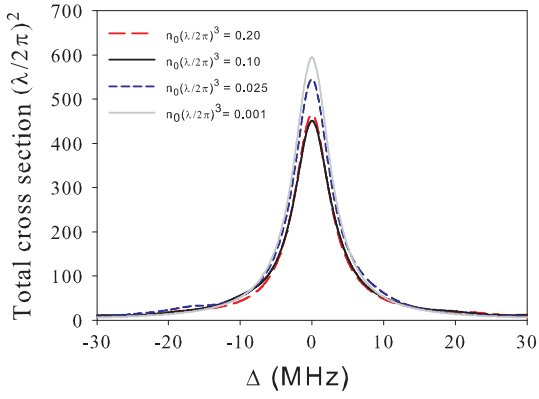


Figure 9. The scattering cross-section calculated microscopically for an ensemble consisting of 100 atoms. Atoms have a spherically symmetrical Gaussian distribution with the peak density varying from $n_0 = 0.001$ to 0.2 and populating only one Zeeman sublevel. (The colour version of this figure is included in the online version of the journal.)

general formalism of the quantum scattering theory previously developed in [27] and present the data for the case of a sample consisting of one hundred atoms. For the typical experimentally attained atomic densities, which are less than $n_o \lesssim 0.1$ in its peak value, in order to resolve the quasi-energy structure, associated with the longitudinal dipole–dipole interaction, it would be enough to take into consideration only a few nearest neighbors in the vicinity of each selected scatterer. This scheme was tested by us on a small number of atoms and it demonstrated reliable convergence, which reduces the number of equations to be solved to $d_e N d_g^{n-1}$, where $n$ is the number of the neighboring atoms retained in the calculation.

In Figure 9 we show the results of our calculations, which were done for $n = 4$ and for all the atoms populating one Zeeman sublevel. Let us point out here again that because

of high degeneracy of the ground state our results cannot be statistically averaged over all the populated initial states. That means we cannot directly compare them on a one-to-one basis either with experiment or with the self-consistently calculated data. Instead, we rely on qualitative comparison among the results.

First, as was explained in [27], because of the presence of elastic Raman scattering channels there is no visible signature of either super- or sub-radiant Dicke-type exciton modes for the $F = 1 \rightarrow F' = 0$ transition. In contrast with $F = 0 \rightarrow F' = 1$ transition (where such states are normally predicted and discussed) in the $F = 1 \rightarrow F' = 0$ case all the resolvent poles are described as the resonances with a typical line width of about $\gamma$. Thus the presence of the cooperative longitudinal and radiative interactions manifest themselves in the smoothed variation of the scattering spectrum associated with disorder and with the configuration dependence. Second, we can point out that because of competition between near and far field interactions the microscopically calculated spectra have an asymmetry in respect to the atomic resonance line. The latter observation is in qualitative agreement with the predictions of the self-consistent model, which were pointed out above.

## 5. Conclusions

We have presented a study of the scattering of light from a cold and highly dense gas of $^{87}$Rb atoms. For radiation tuned in the spectral vicinity of the $F = 1 \rightarrow F' = 0$ hyperfine component of the $D_2$ line, we have studied the atomic density, probe laser detuning and probe laser intensity dependence of the scattered light intensity. The measured time dependence and steady state responses indicate that the light dynamics is strongly affected by Zeeman optical pumping in the lower energy F = 1 hyperfine component. However, for very low probe laser intensities, Zeeman optical pumping can be made negligible; this has allowed for study of the steady state regime in the absence of optical pumping. Of particular interest under these conditions is the line shape of the steady state optical response of the system in comparison with that of the $F = 2 \rightarrow F' = 3$ transition studied in earlier work. Comparison between these results reveals a significantly broader line shape in the case of the $F = 2 \rightarrow F' = 3$ transition. This difference is supported by a self-consistent theory calculation for the two cases, and done under similar density conditions. The comparisons then reveal that the dipole–dipole interaction manifests itself quite differently in differently degenerate atomic transitions, and this difference should be taken into account in considerations of atomic systems at higher densities.

## Acknowledgements

We acknowledge Daniel Havey for informative discussions and contributions to the experimental line shape fitting.

## Funding

We appreciate financial support by the National Science Foundation (Grant Nos. NSF-PHY-0654226 and NSF-PHY-1068159), the Russian Foundation for Basic Research (Grant No. RFBR-CNRS 12-02-91056). D.V.K. would like to acknowledge support from the External Fellowship Program of the Russian Quantum Center (Ref. Number 86). We also acknowledge the generous support of the Federal Program for Scientific and Scientific-Pedagogical Personnel of Innovative Russia for -2013 (Contract No. 14.B37.21.1938). A.S.S. would like to acknowledge support from the charitable foundation 'Dynasty'.

## Notes

1. The entire issue, New J. Phys. 11 (), focuses on recent advances and opportunities in ultracold molecular physics. See particularly, the work of Carr and Ye [61].
2. For an ellipsoidal Gaussian atom distribution of sizes $r_o$ and $z_o$ and peak density $n_o$, $n(r) = n_o \exp(-r^2/2r_o^2 - z^2/2z_o^2)$. The total number of atoms is $N = (2\pi)^{3/2} n_o r_o^2 z_o$ and the peak transverse (longitudinal) optical depth is $b_t = (2\pi)^{1/2} n_o \sigma_o r_o$ ($b_l = (2\pi)^{1/2} n_o \sigma_o z_o$). $\sigma_o$ is the weak field resonance light scattering cross-section. The peak total cross-section is given by
$$\frac{2F'+1}{2F+1}\frac{\lambda^2}{2\pi}.$$

## References

[1] Havey, M.D. *Contemp. Phys.* **2009**, *50*, 587–599.
[2] Metcalf, H.J.; van der Straten, P. *Laser Cooling and Trapping*; Springer: New York, **1999**.
[3] Grimm, R.; Weidemuller, M.; Ovchinnokov, Y. *Adv. Atom., Mol., Opt. Phys.* **2000**, *42*, 95–170.
[4] Pethick, C.J.; Smith, H. *Bose-Einstein Condensation in Dilute Gases*; Cambridge University Press: Cambridge, UK, **2002**.
[5] Giorgini, S.; Pitaevskii, L.P.; Stringari, S. *Rev. Mod. Phys.* **2008**, *80*, 1215–1274.
[6] Bouwmeester, D.; Ekert, A.; Zeilinger, A. *The Physics of Quantum Information*; Springer-Verlag: Berlin, **2001**.
[7] Lukin, M.D. *Rev. Mod. Phys.* **2003**, *75*, 457–472.
[8] Milonni, P.W. *Fast Light, Slow Light, and Left-handed Light*; Taylor and Francis: New York, **2005**.
[9] Fleishhauer, M.; Imamoglu, A.; Marangos, J.P. *Rev. Mod. Phys.* **2005**, *77*, 633–673.
[10] Hau, L.V. *Nat. Photonics* **2008**, *2*, 451–453.
[11] Braje, D.A.; Balic, V.; Yin, G.Y.; Harris, S.E. *Phys. Rev. A* **2003**, *68*, 041801.
[12] Ospelkaus, S.; Pe'er, A.; Ni, K.-K.; Zirbel, J.J.; Neyenhuis, B.; Kotochigova, S.; Julienne, P.S.; Ye, J.; Jin, D.S. *Nat. Phys.* **2008**, *4*, 622–626.
[13] Campbell, G.K.; Ludlow, A.D.; Blatt, S.; Thomsen, J.W.; Martin, M.J.; de Miranda, M.H.; Zelevinsky, T.; Boyd, M.M.; Ye, J.; Diddams, S.A.; Heavner, T.P.; Parker, T.E.; Jefferts, S.R. *Metrologia* **2008**, *45*, 539–548.
[14] Ye, J.; Blatt, S.; Boyd, M.M.; Foreman, S.M.; Hudson, E.R.; Ido, T.; Lev, B.; Ludlow, A.D.; Sawyer, B.C.; Stuhl, B.; Zelinsky, T. *Int. J. Mod. Phys. D* **2007**, *16*, 2481–2494.
[15] Rolston, S. *Physics* **2008**, *1*, 2.
[16] Killian, T.C. *Science* **2007**, *316*, 705–708.
[17] Weidemüller, M.; Zimmermann, C. *Interactions in Ultracold Gases*; Wiley-VCH: Berlin, **2003**.

[18] Fleischhauer, M.; Lukin, M.D. *Phys. Rev. A* **2002**, *65*, 022314.

[19] Dudin, Y.O.; Jenkins, S.D.; Zhao, R.; Matsukevich, D.N.; Kuzmich, A.; Kennedy, T.A.B. *Phys. Rev. Lett.* **2009**, *103*, 020505.

[20] Baudouin, Q.; Mercadier, N.; Guarerra, V.; Guerin, W.; Kaiser, R. *Nat. Phys.* **2013**, *9*, 357–360.

[21] Labeyrie, G. *Mod. Phys. Lett. B* **2008**, *22*, 73–100.

[22] Kupriyanov, D.V.; Sokolov, I.M.; Sukenik, C.I.; Havey, M.D. *Laser Phys. Lett.* **2006**, *3*, 223–243.

[23] Havey, M.D.; Kupriyanov, D.V. *Phys. Scr.* **2005**, *72*, C30–C32.

[24] Kaiser, R.; Havey, M.D. *Opt. Photonics News* **2005**, *16*, 38–43.

[25] Anderson, P.W. *Phys. Rev.* **1958**, *109*, 1492–1505.

[26] Akkermans, E.; Gero, A.; Kaiser, R. *Phys. Rev. Lett.* **2008**, *101*, 103602.

[27] Sokolov, I.M.; Kupriyanova, M.D.; Kupriyanov, D.V.; Havey, M.D. *Phys. Rev. A* **2009**, *79*, 053405; Sheremet, A.S.; Manukhova, A.D.; Larionov, N.V.; Kupriyanov, D.V. *Phys. Rev. A* **2012**, *86*, 043414.

[28] Fofanov, Ya.A.; Kuraptsev, A.S.; Sokolov, I.M.; Havey, M.D. *Phys. Rev. A* **2011**, *84*, 53811.

[29] Sokolov, I.M.; Kupriyanov, D.V.; Havey, M.D. *J. Exp. Theor. Phys.* **2011**, *112*, 246–260.

[30] Wiersma, D.S.; Bartolini, P.; Lagendijk, A.; Righini, R. *Nature* **1997**, *390*, 671–673.

[31] Chabanov, A.A.; Stoytchev, M.; Genack, A.Z. *Nature* **2000**, *404*, 850–853.

[32] Storzer, M.; Gross, P.; Aegerter, C.M.; Maret, G. *Phys. Rev. Lett.* **2006**, *96*, 063904.

[33] Aegerter, C.M.; Maret, G. *Coherent backscattering and Anderson localization of light*, in *Progress in Optics 52*; Elsevier: Amsterdam, **2009**; p. 1–62.

[34] Scully, M.O. *Phys. Rev. Lett.* **2009**, *102*, 143601.

[35] Svidzinsky, A.A.; Chang, J.; Scully, M.O. *Phys. Rev. Lett.* **2008**, *100*, 160504.

[36] Froufe-Pérez, L.; W. Guerin, W.; Carminati, R.; Kaiser, R. *Phys. Rev. Lett.* **2009**, *102*, 173903.

[37] Bienaime, T.; Bachelard, R.; Piovella, N.; Kaiser, R. *Fortschr. Phys.* **2012**, doi:10.1002/prop.201200089.

[38] Bienaime, T.; Petruzzo, M.; Bigerni, D.; Piovella, N.; Kaiser, R. *J. Mod. Opt.* **2011**, *58*, 1942–1950.

[39] Bux, S.; Lucioni, E.; Bender, H.; Bienaime, T.; Lauber, K.; Stehle, C.; Zimmermann, C.; Slama, S.; Courteille, Ph.W.; Piovella, N.; Kaiser, R. *J. Mod. Opt.* **2010**, *57*, 1841–1848.

[40] Bienaime, T.; Bux, S.; Lucioni, E.; Courteille, Ph.W.; Piovella, N.; Kaiser, R. *Phys. Rev. Lett.* **2010**, *104*, 183602.

[41] Courteille, Ph.W.; Bux, S.; Lucioni, E.; Lauber, K.; Bienaime, T.; Kaiser, R.; Piovella, N. *Eur. Phys. J. D* **2010**, *58*, 69–73.

[42] Cao, H. *Lasing in Disordered Media*, in *Progress in Optics 45*, Elsevier: Amsterdam, **2003**.

[43] Wiersma, D.S. *Nat. Phys.* **2008**, *4*, 359–367.

[44] Conti, C.; Fratalocchi, A. *Nat. Phys.* **2008**, *4*, 794–798.

[45] Froufe-Pérez, L.; Guerin, W.; Carminati, R.; Kaiser, R. *Phys. Rev. Lett.* **2009**, *102*, 173903.

[46] Guerin, W.; Mercadier, N.; Brivio, D.; Kaiser, R. *Opt. Express* **2009**, *17* (14), 11236–11245.

[47] Guerin, W.; Mercadier, N.; Michaud, F.; Brivio, D.; Froufe-Pérez, L.S.; Carminati, R.; Eremeev, V.; Goetschy, A.; Skipetrov, S.E.; Kaiser, R. *J. Opt. A* **2010**, *12*, 024002.

[48] Nielsen, M.A.; Chuang, I.L. *Quantum Computation and Quantum Information;* Cambridge University Press: Cambridge, UK, **2000**; p. 517.

[49] Briegel, H.-J.; Dur, W.; Cirac, J.I.; Zoller, P. *Phys. Rev. Lett.* **1998**, *81*, 5932–5935.

[50] Duan, L.-M.; Lukin, M.D.; Cirac, J.I.; Zoller, P. *Nature* **2001**, *414*, 413–418.

[51] Bienaime, T.; Piovella, N.; Kaiser, R. *Phys. Rev. Lett.* **2012**, *108*, 123602.

[52] Datsyuk, V.M.; Sokolv, I.M.; Kupriyanov, D.V.; Havey, M.D. *Phys. Rev. A* **2008**, *77*, 033823.

[53] Datsyuk, V.M.; Sokolv, I.M.; Kupriyanov, D.V.; Havey, M.D. *Phys. Rev. A* **2006**, *74*, 043812.

[54] Sokolv, I.M.; Kupriyanov, D.V.; Olave, R.G.; Havey, M.D. *J. Mod. Opt.* **2010**, *57*, 1833–1840.

[55] Gerasimov, L.V.; Sokolv, I.M.; Kupriyanov, D.V.; Olave, R.G.; Havey, M.D. *J. Opt. Soc. Am. B* **2011**, *28*, 1459–1466.

[56] Gerasimov, L.V.; Sokolv, I.M.; Kupriyanov, D.V.; Havey, M.D. *J. Phys. B: At. Mol. Opt. Phys.* **2012**, *45*, 124012.

[57] Fofanov, Ya.A.; Kuraptsev, A.S.; Sokolv, I.M.; Havey, M.D. *Phys. Rev. A* **2013**, *87*, 063839.

[58] Balik, S.; Win, A.L.; Havey, M.D.; Sokolv, I.M.; Kupriyanov, D.V. *Phys. Rev. A* **2013**, *87*, 053817.

[59] Balik, S.; Win, A.L.; Havey, M.D. *Phys. Rev. A* **2009**, *80*, 023404.

[60] Sokolv, I.M.; Kuraptsev, A.S.; Kupriyanov, D.V.; Havey, M.D.; Balik, S. *J. Mod. Opt.* **2013**, *60*, 50–56.

[61] Carr, L.D.; Ye, J. *New J. Phys.* **2009**, *11*, 055009.